Graphical Abstract

Limited Visual Range in the Social Force Model: Effects on Macroscopic and Microscopic Dynamics

Ander García, Dariel Hernández-Delfín, Dae-Jin Lee, Marco Ellero

Highlights

Limited Visual Range in the Social Force Model: Effects on Macroscopic and Microscopic Dynamics

Ander García, Dariel Hernández-Delfín, Dae-Jin Lee, Marco Ellero

- Bottleneck flow and fundamental diagram in the social force model
- Parameter-sensitivity analysis in three social force specifications
- Effect of limited visual range on individual and global dynamics
- Reproduction of macroscopic empirical data if limited visual range is considered
- Study of collision avoidance in the microscopic and macroscopic scale
- Lane formation in moderately crowded bidirectional pedestrian flows

Limited Visual Range in the Social Force Model: Effects on Macroscopic and Microscopic Dynamics

Ander García[a,b], Dariel Hernández-Delfín[a], Dae-Jin Lee[a,c], Marco Ellero[a,d,e]

[a]*Basque Center for Applied Mathematics (BCAM), Alameda Mazarredo 14, Bilbao, 48009, Spain*
[b]*Department of Mathematics, University of the Basque Country UPH/EHU, P.O. 644, Bilbao, 48080, Spain*
[c]*IE University - School of Science and Technology), Paseo de la Castellana 259, Madrid, 28029, Spain*
[d]*IKERBASQUE, Basque Foundation for Science, Calle María Diaz de Haro 3, Bilbao, 48013, Spain*
[e]*Zienkiewicz Center for Computational Engineering (ZCCE), Swansea University, Bay Campus, Swansea SA1 8EN, Swansea, SA1 8EN, United Kingdom*

Abstract

The Social Force Model has been widely used to simulate pedestrian dynamics. Its simplicity and ability to reproduce some collective patterns of behavior make it an adequate tool in the field of pedestrian dynamics. However, its ability to reproduce common macroscopic empirical results, such as pedestrian flows through a bottleneck and the speed-density fundamental diagram, has scarcely been studied. In addition, the effect of each parameter of the model on the dynamics of the system has rarely been shown. In this contribution, a comprehensive parameter-sensitivity analysis in the social force model is provided, and an optimal set is introduced, capable of reproducing both macroscopic experimental flow data and collision avoidance between pedestrians in simple trajectories on the microscopic scale. We show that the incorporation of asymmetric visual range models in the inter-pedestrian interactions is required for quantitative agreement. The model is also capable of showing collision avoidance in simple pedestrian trajectories and lane formation in non-crowded bidirectional pedestrian flows.

Keywords: Social Force Model, Limited Visual Range, Flow Through a Bottleneck, Fundamental Diagram, Collision Avoidance, Bidirectional Flows

Preprint submitted to Physica A

1. Introduction

The interest in pedestrian dynamics has increased in the last decades due to the importance of predicting the motion of pedestrian crowds. It becomes especially relevant for pedestrian safety and the design of facilities in scenarios where a high number of people are involved.

One of the most widely employed mathematical models is the so-called Social Force Model (SFM), introduced originally by Helbing and Molnár in 1995 [1]. The first version of the model consisted of two kinds of forces: a driving force to induce the pedestrians to move towards their desired destination and inter-pedestrian distance-dependent repulsion or attraction forces to avoid unphysical clusters or simulate social groups. Although simple, the model showed satisfactory results, as it reproduced lane formation (LF) in bidirectional pedestrian flows (BPF) and arch formation before bottlenecks. In a series of later publications, Helbing and collaborators included contact forces and simulated evacuation of pedestrians through narrow gates [2], as well as more complex versions of the repulsive forces, e.g., including the anisotropy of pedestrian interactions to mimic limited visual range [3, 4]. In the last two mentioned contributions, parameter calibration was done by comparing experimental and simulated trajectories of pedestrians. A similar analysis was also performed by other authors [5]. One of the most popular studies performed with either the SFM or its modified versions is the simulation of crowd evacuations. Researchers have studied the characteristics of pedestrian evacuations in virtual geometries with a single exit [6, 7] or multiple exits [8, 9, 10] and in real subway geometries [11, 12, 13]. Despite the large number of computational studies in the SFM, researchers have scarcely utilized two of the most critical macroscopic empirical results, i.e., bottleneck flows (BF) and the speed-density fundamental diagram (FD), in validating the models. Hence, the knowledge about the reproducibility of these macroscopic empirical results by the existing models is limited; even though BF provides valuable information for evacuations by measuring the number of pedestrians exiting the bottleneck during the process, and FD shows how the speed of pedestrians is reduced with increasing density, and therefore they should represent an important part of the validation stage [14].

In BF experiments, often carried out at universities with volunteers, participants are located in a corridor and asked to exit through a gate at one of the extremes. In all experiments, trials are performed with different widths of the gate to obtain a relation between the flow and the gate width. Some au-

thors have used this outcome as a benchmark to assess their models [15, 16]. Here, we compare our numerical BF results with the data from Rupprecht et al. [17], Liao et al. [18], Müller [19], Liu et al. [20], Kretz et al. [21], Seyfried et al. [22], Nagai et al. [23], and Muir et al. [24].

The speed-density FD relates the average velocity of pedestrians with the density. We compare our numerical results with the experimental data from the following five references, in which results are obtained in experiments performed at universities [25, 26], measuring walking speeds of people [27, 28] or introducing an equation based on empirical results to explain the fundamental diagram [29]. The diagram shows a heterogeneous behavior of pedestrians, as factors such as gender, age, culture, motivation, or type of facility affect people's velocity [30]. Regarding the SFM, Parisi et al. [31] showed that a modification of it, consisting of the introduction of a respect area for each pedestrian i such that, in case of being occupied by another particle, the desired velocity of pedestrian i is set to zero, could reproduce empirical fundamental diagrams. Furthermore, Bassoli and Vincenzi [32] showed that the SFM could also reproduce results from fundamental diagrams if the anisotropic nature of pedestrian interactions is considered; however, neither a BF nor a microscopic analysis was performed. In other models, authors have used the FD to evaluate the realism of numerical results [33, 34, 35, 36, 37, 38, 15, 16].

In this contribution, we explore the ability of three typical specifications of the SFM to reproduce the aforementioned experimental results. We show a detailed analysis of the effect of some of the parameters of the model in the dynamics and introduce a set of parameters capable of reproducing both BF and FD. We also study collision avoidance in simple pedestrian trajectories and macroscopic scenarios, and lane formation in bidirectional pedestrian flows. The paper is organized as follows. First, we introduce the mathematical aspects of the SFM. Secondly, we explain the details of our simulations. Thirdly, we analyze the effect of the parameters on the dynamics and compare the numerical results of each specification with macroscopic experimental data. Then, we show some collision trajectories using the parameters fitted in the macroscopic analysis and assess the collision avoidance in macroscopic scenarios where many people are involved. Finally, we study the lane formation in bidirectional pedestrian flows for several values of the global pedestrian density.

2. The Social Force Model

The Social Force Model (SFM) is a mathematical model to simulate pedestrian dynamics based on Newton's second law. Depending on the position of the pedestrian i at time t, $\mathbf{r}_i(t)$, each pedestrian i has a desired velocity $\mathbf{v}_i^0(\mathbf{r}_i(t)) = v_i^0 \mathbf{e}_i(\mathbf{r}_i(t))$, where v_i^0 is the desired speed magnitude, and $\mathbf{e}_i(\mathbf{r}_i(t))$ is the unit vector pointing towards the desired direction of motion for each pedestrian. The force associated with the pedestrians' desire to move in the direction of $\mathbf{e}_i(\mathbf{r}_i(t))$ is the driving force, defined as

$$\mathbf{f}_i^{\mathrm{d}}(\mathbf{r}_i(t)) = m\frac{\mathbf{v}_i^0(\mathbf{r}_i(t)) - \mathbf{v}_i(t)}{\tau}, \tag{1}$$

where m is the mass of each pedestrian i, $\mathbf{v}_i(t)$ their actual velocity at time t, and τ is the relaxation time to adapt the actual velocity to the desired one.

Together with the driving force, the model includes a repulsive social force to avoid close collisions between agents and obstacles. Here, obstacles are considered to be wall particles or other pedestrians. The force is described through the function $\mathbf{f}_{ij}^{\mathrm{r}}(\mathbf{r}_{ij}(t))$, where $\mathbf{r}_{ij}(t) = \mathbf{r}_i(t) - \mathbf{r}_j(t)$ is the vector pointing from the center of obstacle j to the center of pedestrian i. The two most used versions of the repulsive social force are the circular specification,

$$\mathbf{f}_{ij}^{\mathrm{r}} = Ae^{-\frac{r_{ij}}{B}}\mathbf{u}_{ij}, \tag{2}$$

and the elliptical specification,

$$\mathbf{f}_{ij}^{\mathrm{r}} = Ae^{-\frac{b_{ij}}{B}} \cdot \frac{\|\mathbf{r}_{ij}\| + \|\mathbf{r}_{ij} - \mathbf{y}_{ij}\|}{2b_{ij}} \cdot \frac{1}{2}\left(\mathbf{u}_{ij} + \frac{\mathbf{r}_{ij} - \mathbf{y}_{ij}}{\|\mathbf{r}_{ij} - \mathbf{y}_{ij}\|}\right), \tag{3}$$

where A and B are the intensity and range of the social force, respectively, $\mathbf{u}_{ij} = \frac{\mathbf{r}_{ij}}{\|\mathbf{r}_{ij}\|}$ is the unit vector pointing from obstacle j to pedestrian i, and $\mathbf{y}_{ij} = (\mathbf{v}_j - \mathbf{v}_i)\Delta T$, where ΔT is a temporal parameter to model the anticipation of pedestrians to the obstacle. Unlike the circular specification described by eq. (2), the elliptical specification, as its name indicates, possesses an elliptical shape with

$$2b_{ij} = \sqrt{\left(\|\mathbf{r}_{ij}\| + \|\mathbf{r}_{ij} - \mathbf{y}_{ij}\|\right)^2 - \|\mathbf{y}_{ij}\|^2} \tag{4}$$

as the semi-minor axis of the ellipse. These two specifications of the social force have the symmetry $\mathbf{f}_{ij}^{\mathrm{r}} = -\mathbf{f}_{ji}^{\mathrm{r}}$ under pedestrian index swap, therefore

conserving the total linear momentum. Strictly speaking, the previous relation is an anti-symmetry; however, for the sake of clarity, we refer to it as symmetric to distinguish it from the asymmetric interaction discussed later. Nevertheless, real social interactions among pedestrians are intrinsically asymmetric due to their limited visual range. This fact can be included in simulations by multiplying the repulsive force $\mathbf{f}_{ij}^{\mathrm{r}}$ by a weight factor that considers how people react to obstacles depending on their position with respect to pedestrians' visual range, e.g., pedestrians tend to socially interact more strongly with others at a forward position rather than behind. Assuming that the heading direction is aligned with the current velocity vector $\mathbf{v}_i$, the mathematical expression for the weight factor is [4]:

$$w(\varphi_{ij}) = \lambda + (1-\lambda)\frac{1+\cos(\varphi_{ij})}{2} \tag{5}$$

where $\lambda \in [0,1]$ and φ_{ij} is the angle between $\mathbf{v}_i$ and $\mathbf{r}_{ji} = -\mathbf{r}_{ij}$:

$$\cos(\varphi_{ij}) = \frac{\mathbf{v}_i}{||\mathbf{v}_i||} \cdot \frac{\mathbf{r}_{ji}}{||\mathbf{r}_{ji}||} \tag{6}$$

This prefactor is a cardioid function, and Figure 1 displays it for different values of the parameter λ. We apply this weight only for inter-pedestrian interactions. If applied to pedestrian-wall interactions, the resulting wall social force would have a component in the direction parallel to the wall, and pedestrians would artificially walk slower.

In addition, when pedestrians, simulated as disks of radius R_i, come closer than the sum of their radii $R_{ij} = R_i + R_j$, contact forces $\mathbf{f}_{ij}^{\mathrm{c}}(\mathbf{r}_{ij}(t))$ are activated. These are divided into two different contributions: a body force counteracting compression,

$$\mathbf{f}_{ij}^{\mathrm{B}}\left(\mathbf{r}_{ij}(t)\right) = H\left(R_{ij} - r_{ij}\right)\mathbf{u}_{ij}, \tag{7}$$

and a shear force that simulates friction,

$$\mathbf{f}_{ij}^{\mathrm{S}}\left(\mathbf{r}_{ij}(t)\right) = \gamma\left(R_{ij} - r_{ij}\right)\left(\mathbf{v}_{ji}\cdot\mathbf{t}_{ij}\right)\mathbf{t}_{ij}, \tag{8}$$

where H and γ are the compression and shear parameters, respectively, $\mathbf{v}_{ji} = \mathbf{v}_j - \mathbf{v}_i$ and $\mathbf{t}_{ij} = (-u_{ij}^{(\mathrm{y})}, u_{ij}^{(\mathrm{x})})$ is the unitary vector in the tangential direction (here, the upper index indicates the x and y components of the unitary vector $\mathbf{u}_{ij}$). The total contact force is, therefore,

$$\mathbf{f}_{ij}^{\mathrm{c}}(\mathbf{r}_{ij}(t)) = \mathbf{f}_{ij}^{\mathrm{B}}\left(\mathbf{r}_{ij}(t)\right) + \mathbf{f}_{ij}^{\mathrm{S}}\left(\mathbf{r}_{ij}(t)\right). \tag{9}$$

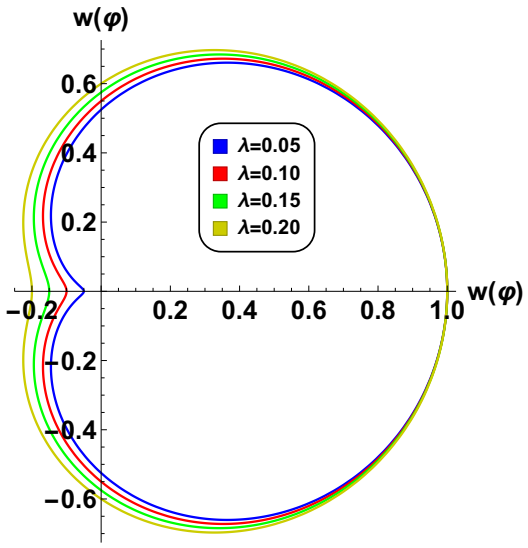

Figure 1: Polar plot of $w(\varphi_{ij})$ (eq. (5)) as a function of φ_{ij} for several λ values.

Thus, the final acceleration equation for pedestrian i reads:

$$m\frac{\mathrm{d}\mathbf{v}_i(t)}{\mathrm{d}t} = \mathbf{f}_i^{\mathrm{d}} + \sum_j \mathbf{f}_{ij}^{\mathrm{r}} + \sum_j \mathbf{f}_{ij}^{\mathrm{c}}, \tag{10}$$

which, together with $\mathrm{d}\mathbf{r}_i(t)/\mathrm{d}t = \mathbf{v}_i(t)$, define the dynamics of the system.

3. Simulation Framework and Geometrical Specifications

We perform simulations to study the macroscopic and microscopic behavior of pedestrians, simulated as disks of diameter $D_{\mathrm{ped}} = 0.5$ m. Wall particles are also simulated using disks of diameter $D_{\mathrm{w}} = 0.5$ m, and the distance between their center is 0.25 m. Hence, the successive disks forming the wall overlap. The reason to have overlapping wall particles is mainly to avoid the diffusion of pedestrians through walls in high-density scenarios, where the pressure on walls can reach large values. In the macroscopic study, we have focused on the mentioned bottleneck flows (BF) and speed-density fundamental diagram (FD). In the former, 300 pedestrians are located in a 25 m long and 5 m wide corridor, randomly distributed in the region $x \in (0, 13)$ m before the exit, which is located at $x = 16$ m (Fig. 2). The desired direction of pedestrians points towards the gate, and for each set of parameters

of the model, we have performed five different runs, in which the width of the gate b varies from $b = 0.8$ m to $b = 2.4$ m in steps of 0.4 m. To measure the flow, we initialize a counter that measures how many people $N(t)$ have crossed the exit at time t. The flow-width relation is obtained by linear regression of the data, excluding the first and last 15 pedestrians in order to avoid transient effects. Figure 2 shows a snapshot of the BF simulation.

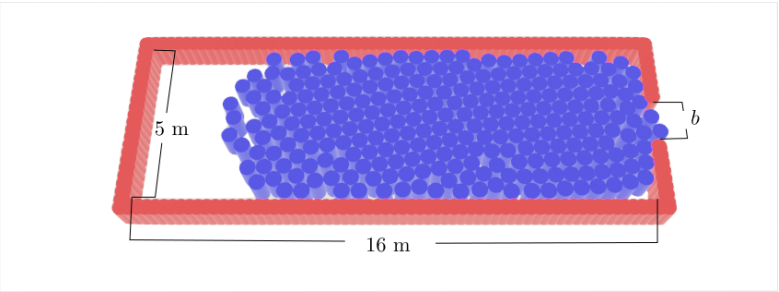

Figure 2: Snapshot of the BF simulation: pedestrians in blue, wall particles in red. b represents the width of the exit.

Secondly, to evaluate the FD, for each set of the parameters of the model, we perform eight runs, varying in each of them the density of the system. The density is the ratio between the total number of people and the area of the corridor (125 m^2), and we simulate flows for pedestrian densities increasing from moderate $\rho = 0.5$ m^{-2} to highly packed $\rho = 4.0$ m^{-2} in steps of 0.5 m^{-2}. The average velocity of all pedestrians is calculated in each time step t, and once the system is in a steady state, we take the time average. In FD simulations, the desired direction of pedestrians is parallel to the walls of the corridor, and agents are initially located in random positions throughout the corridor (25m $\times$ 5m). We also establish periodic boundary conditions: pedestrians exiting the corridor from the right will re-enter from the left. Figure 3 illustrates a snapshot of the FD simulation.

Afterwards, we conduct a microscopic study to assess the ability of pedestrians to avoid obstacles or other pedestrians. We examine the trajectories of pedestrians in three cases. In the first experiment, a pedestrian walks towards a fixed obstacle; in the second, two pedestrians walk in opposite directions, one towards the other. In the third case, a faster pedestrian overtakes a slower one. We evaluate the ability of each set of parameters to avoid collision, and we analyze the shape of the trajectory. The microscopic study is complemented with a macroscopic analysis of collision avoidance, in which

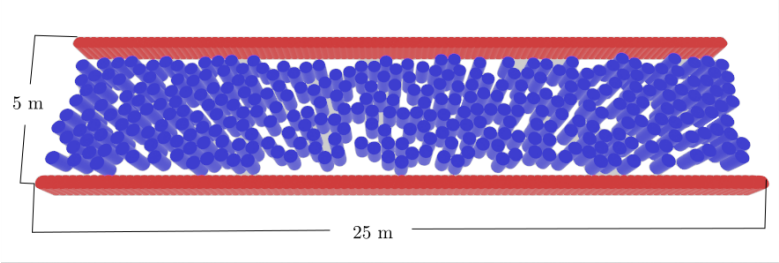

Figure 3: Snapshot of the FD simulation: pedestrians in blue, wall particles in red.

we focus on the time average of the number of contacts per pedestrian for several values of the global pedestrian density.

Finally, we study the onset of lane formation in bidirectional pedestrian flows. To focus only on pedestrian interactions, we slightly modify the geometry of the system: walls are removed, and periodic boundary conditions are established in both the longitudinal and transversal directions of the corridor. Pedestrians walking in opposite directions are located initially in random positions in two waiting areas at the extremes of the corridor, as shown in Figure 4. To ensure that agents have enough space to accelerate to their desired velocity before interacting with pedestrians in counterflow, we increase the size of the periodic corridor to $(40\text{m} \times 15\text{m})$. We consider different global pedestrian densities ρ, and for each value of ρ, we run ten simulations with different initial positions of the pedestrians to obtain a probability of lane formation as a function of the global density.

3.1. SFM Parameter Choice

Four parameters of the model are kept constant in all simulations: the desired speed v_i^0 of pedestrians, sampled from a Gaussian distribution with mean 1.45 m/s and standard deviation of 0.23 m/s, following [39]; the parameter $\lambda = 0.1$ for the weight factor $w(\varphi_{ij})$, following [3]; the mass $m = 80$ kg for every pedestrian, and the range of the social force $B = 0.6$ m. Furthermore, for calculation efficiency, we establish a cut-off radius to the social force of $R_{\text{cut}} = 4.5$ m.

In macroscopic simulations, our analysis focuses on the three parameters that characterize each force term: the social force intensity, A, and the compression and shear parameters, H and γ, respectively. We show the results of several simulations in which we vary one parameter among A, H, and γ,

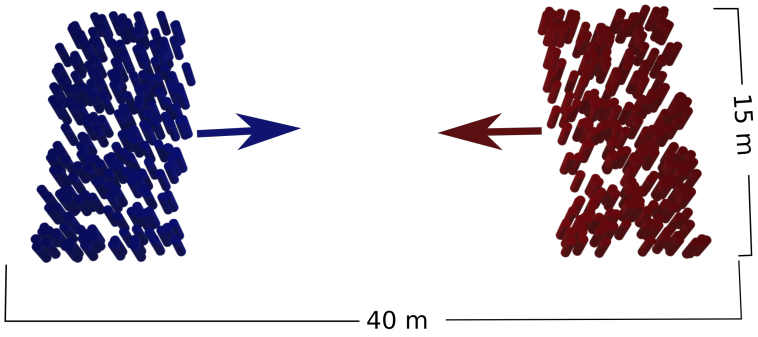

Figure 4: Snapshot of the LF simulation: red-colored pedestrians walk to the left, whereas blue-colored pedestrians, to the right.

and keep the rest constant with the aim of determining the effect of each one. The selected values are shown in Table 1. When the effect of other parameters is studied, we keep the other two force parameters constant as follows: $A_0 = 45$ N, $H_0 = 1.2 \times 10^4$ kg s^{-2}, and $\gamma_0 = 1.5 \times 10^4$ kg m^{-1} s^{-1}.

Value	A	H	γ
Low: $\downarrow$	3.0×10^1	9.0×10^3	1.0×10^4
Medium: $\rightarrow$	4.5×10^1	1.2×10^4	1.5×10^4
High: $\uparrow$	6.0×10^1	1.5×10^4	2.0×10^4

Table 1: Values of the parameters in macroscopic simulations. The units are: A (N), H (kg s^{-2}), and γ (kg m^{-1} s^{-1}).

In microscopic simulations, τ and ΔT are also varied among $\tau = 1,\ 2,$ and 3 s and $\Delta T = 0, 1.0$ and 1.5 s, keeping them constant and equal to $\tau_0 = 1$ s and $\Delta T_0 = 1$ s when the effect of the other parameter is studied. In both macroscopic collision avoidance and bidirectional flow simulations, we use the parameters that show the best results in the aforementioned simulations.

4. Results and Discussion

In this section, we show the effect of each of the studied parameters in macroscopic and microscopic dynamics by differentiating between the circu-

lar, elliptical, and asymmetric elliptical specifications of the social force, and we introduce a set of parameters that fits both BF and FD results. Then, we use that combination of force parameters in the microscopic and macroscopic collision avoidance analysis.

4.1. Macroscopic Flow Dynamics

4.1.1. Flow Through a Bottleneck (BF)

Figure 5 shows bottleneck flow results for the three social force specifications and different values of each parameter. The effect of the intensity of the social force depends on the specification: for the circular and elliptical specifications, increasing values of A accelerate the flow, whereas for the asymmetric model, the flow rate is reduced as A increases, as pictured in Figure 5 (a). It is clear that the asymmetric model does the best job of capturing BF data.

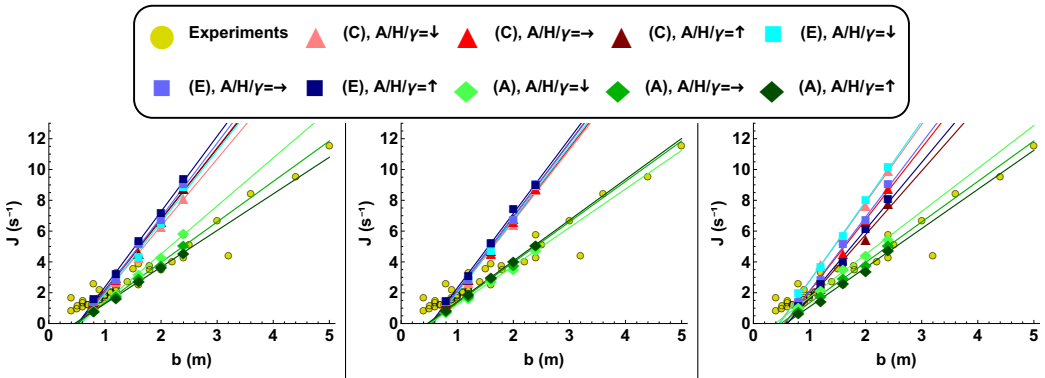

Figure 5: BF in the circular (C), elliptical (E) and asymmetric elliptical (A) specifications, focusing of the effect of: (a) Social force intensity A, (b) Compression parameter H, and (c) Shear parameter γ. The values of each parameter are specified in Table 1.

To understand the difference between models, we calculate the average social and contact force in the x-direction (longitudinal coordinate of the corridor) per pedestrian, $\overline{f}^r$ and $\overline{f}^c$, respectively:

$$\overline{f}^r = \langle \mathbf{f}_{ij}^{r\,(x)} \rangle = \frac{1}{N_{\text{ped}}} \sum_{i=1}^{N_{\text{ped}}} \sum_{j=1}^{N_{\text{obs}}} \mathbf{f}_{ij}^{r\,(x)}$$

and

$$\overline{f}^{c} = \langle \mathbf{f}_{ij}^{c\,(x)} \rangle = \frac{1}{N_{\text{ped}}} \sum_{i=1}^{N_{\text{ped}}} \sum_{j=1}^{N_{\text{obs}}} \mathbf{f}_{ij}^{B(x)} + \mathbf{f}_{ij}^{S(x)},$$

where N_{ped} is the total number of pedestrians and $N_{\text{obs}} = N_{\text{wall}} + N_{\text{ped}}$ the total number of obstacles, i.e., the number of wall particles (N_{wall}) or other individuals (N_{ped}) that pedestrian i is interacting with. Figures 6 and 7 show, respectively, the average social and contact forces as a function of time. The main difference between symmetric and asymmetric models is that in the former, contact forces are dominant, whereas in the latter, it is the social force which dominates the dynamics. By definition, in symmetric models, $\mathbf{f}_{ij}^{r} = -\mathbf{f}_{ji}^{r}$; therefore, pedestrian-pedestrian interactions (both social and contact) do not contribute to the average. The resulting averages in Figures 6 and 7 come from pedestrian-wall interactions, which do not cancel since we are not considering the force over walls in the sum. In this case, the magnitude of contact forces in the x-direction determines the dynamics, as they are dominant, and as A is increased, the repulsive screening is more effective and the magnitude of $\overline{f}^{c}$ decreases. Higher social force intensity, therefore, contributes to avoiding contacts; hence, the flow rate is increased. Contrary to this case, in the asymmetric model $\mathbf{f}_{ij}^{r} \neq -\mathbf{f}_{ji}^{r}$ due to the effect of the visual weight function $w(\varphi_{ij})$. Here, the repulsion from pedestrians above is greater than the repulsion from individuals below, and the contribution of pedestrian-pedestrian social interaction does not cancel on average. As a result, linear momentum is not conserved and $\overline{f}^{r}$ is greater than in symmetric cases, and consequently, it dominates the flow. As A increases, so does $\overline{f}^{r}$ (in magnitude), and although the magnitude of contact forces is reduced (Fig. 7), the social repulsion overwhelms it, leading to a decrease in the flow rate.

In the case of contact forces, the behavior is the same for the three specifications: increasing values of the compression H and decreasing values of the shear γ accelerate the flow, and vice-versa, as shown, respectively, in Figures 5 (b) and (c). We have energy dissipation and hence a reduction in pedestrians' velocity if contacts happen. This energy dissipation increases with the shear parameter γ, hence the reduction in the flow rate as it increases. On the other hand, the larger the compression parameter H, the better contacts are counteracted, i.e., they occur over a shorter time, and the motion will be consequently faster. Apart from that, focusing on Figure 5 (c), it is possible to see that, although the effect of contact is the same

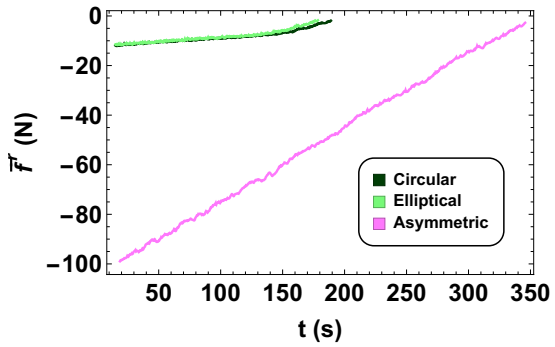

Figure 6: $\overline{f}^r$, as a function of time, for $b = 0.8$ m and $A = 60$ N and the three force specifications. The magnitude of the social force is greater in the asymmetric case, hence, the longer time of evacuation.

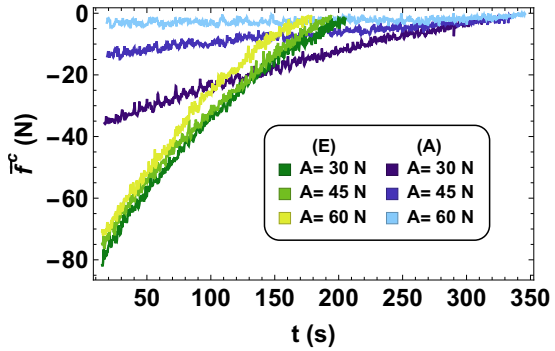

Figure 7: $\overline{f}^c$, as a function of time, for the elliptical (E) and asymmetric (A) specifications, with $b = 0.8$ m. As A increases, $\overline{f}^c$ decreases in magnitude; therefore, the resulting contact force against the direction of motion is reduced.

in the three specifications, an increasing friction γ has a more considerable effect on symmetric force specifications than in the asymmetric case. This is because of the already mentioned effect of the social force intensity, which slows down the system more effectively than in the symmetric case.

Finally, for the studied set of parameters, symmetric specifications can correctly reproduce the data for the smallest exit widths $b = 0.8$ and 1.2 m, but numerical results deviate for the widest gates, significantly overestimating the slope of the flow-gate relation. Conversely, the results for the asymmetric elliptical model are much closer to the real for $b = 1.6,\ 2.0$ and 2.4 m, and for the two smallest widths, simulations are very close to experi-

mental data, making the slope of the regression curve in good agreement with the empirical data. These results suggest favoring the use of the asymmetric model rather than symmetric ones in the reproduction of flow data, thanks to the unbalanced social repulsion forces due to the finite visual range.

4.1.2. Fundamental Diagram

Figure 8 shows the fundamental diagram for the three social force specifications and different values of each parameter. The effect of the social force is negligible or slight in the symmetric models (circular and elliptical), whereas, in the asymmetric model, the slowdown of the system with increasing values of A is evident, as shown in Figure 8 (a).

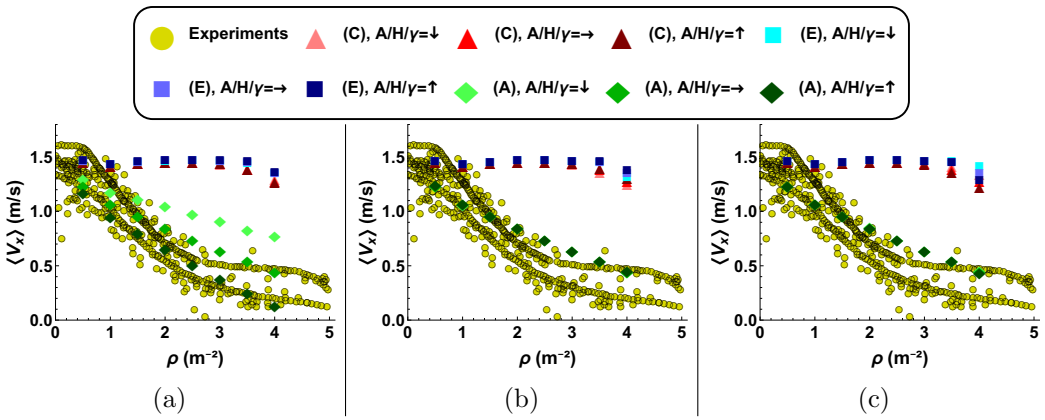

Figure 8: FD in the circular (C), elliptical (E) and asymmetric elliptical (A) specifications, focusing of the effect of: (a) Social force intensity A, (b) Compression parameter H, and (c) Shear parameter γ. The values of each parameter are specified in Table 1.

As in the previous section, we calculate the average social force in the x-direction over each pedestrian, but now we take the time average at the steady state, and show it as a function of the pedestrian density in Figure 9. For symmetric models, the mean is close to zero due to the cancellation of pair pedestrian-pedestrian and pedestrian-wall forces, whereas in the asymmetric case, it increases in magnitude with pedestrian density ρ. In symmetric models, social repulsion is independent of the position of the pedestrian, whereas in the asymmetric version, repulsion from people in front of an individual repels him/her more, as sketched in Figure 10. Moreover, as density or A

increases, so will the average social repulsion, and as a consequence, the flow rate is reduced.

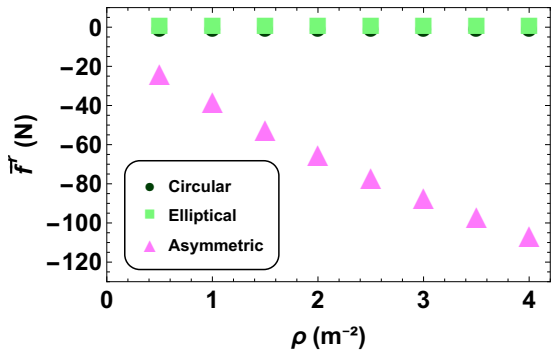

Figure 9: $\overline{f}^r$, averaged in time, as a function of pedestrian density. In symmetric specifications, the average is close to zero, whereas in the asymmetric interaction, it becomes more negative with increasing density.

On the other hand, in the symmetric specifications, the effect of contact forces is negligible for dilute and intermediate density scenarios ($\rho < 3.0$ m^2), as most of the contacts with walls can still be avoided via social repulsion. However, above those values of ρ, more contacts with walls occur and smaller H and greater γ lead to smaller average velocity $\langle v_x \rangle$ in the system. On the contrary, for the chosen set of parameters, contact forces do not affect the flow in the asymmetric model, again due to the dominance of social forces in slowing down the flow.

In view of these results, the combined macroscopic analysis (BF and FD) shows that the asymmetric model must be used to correctly reproduce empirical data. The fit in both BF and FD is good for the chosen set of parameters, whereas, in symmetric models, the flow is too fast in both simulations as the social force is unable to decelerate pedestrians.

4.1.3. Effect of the size of pedestrians

In the previous analysis, with the purpose of keeping the model simple and focusing on the effect of individual parameters on the dynamics, the diameter of pedestrians was kept constant and equal to $D_{\text{ped}} = 0.5$ m (same as wall particles forming the environment). In reality, there is a certain variability of D_{ped}. Thus, we extend our analysis by looking at the effect of the size of pedestrians in BF and FD. We run simulations in the asymmetric elliptical specification, varying pedestrians' size between $D_{\text{ped}} = 0.40,\ 0.45$

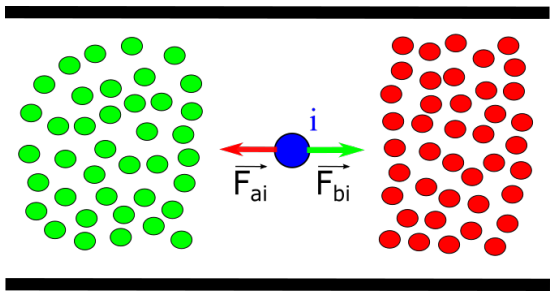

Figure 10: Sum of social repulsive forces on pedestrian i (blue) from people below (green) and above (red). In symmetric specifications, $\|\vec{F}_{ai}\| \approx \|\vec{F}_{bi}\|$, and the resulting total repulsive force oscillates around zero. Contrary to this, in the asymmetric specification, $\|\vec{F}_{ai}\| >> \|\vec{F}_{bi}\|$, and the resulting total social force opposes the driving force.

and 0.50 m. Since we are trying to obtain the best fit of empirical data, we choose the force parameters accordingly. Looking at the FD in Figure 8 (a), $A = 60$ N offers the best fit to empirical data. On the other hand, contact force parameters slightly modify the dynamics; hence, we choose the intermediate values of $H = 1.2 \times 10^4$ kg s^{-2} and $\gamma = 1.5 \times 10^4$ kg m^{-1} s^{-2}. Moreover, as in the last simulations, τ and ΔT will be constant and equal to 1 s.

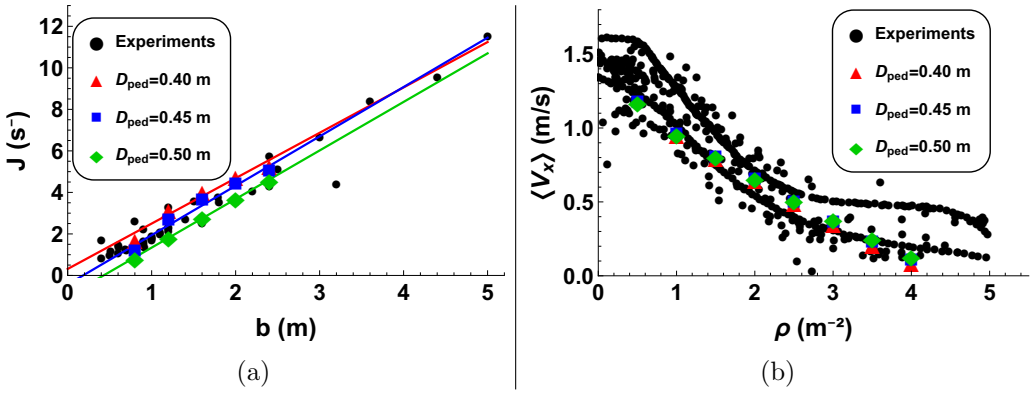

(a) (b)

Figure 11: (a) Bottleneck flows for pedestrians of diameter $D_{\text{ped}} = 0.40,\ 0.45$ and 0.50 m. (b) Fundamental diagram for pedestrians of diameter $D_{\text{ped}} = 0.40,\ 0.45$ and 0.50 m.

Figure 11 (a) shows the results for BF. If pedestrians are smaller, contacts among them are reduced and it is easier for them to walk through the gate;

hence, the flow rate through the exit is accelerated. We have a perfect fit of the data when $D_{\text{ped}} = 0.40$ and 0.45 m. For $D_{\text{ped}} = 0.50$ m, the flow is not fast enough for $b = 0.8$ and 1.2 m gate widths.

On the other hand, the fundamental diagram is plotted in Figure 11 (b). As explained in the fundamental diagram analysis (see section 4.1.2), contact forces barely change the flow through the channel. When the density is low, contacts as less likely to occur, whereas when the density is higher, their effect is negligible as it is proportional to the (slow) relative velocity. Since the main effect of the size of pedestrians will be related to the contacts between them, it is reasonable to have an unaltered FD. Finally, the FD data is also well reproduced for $D_{\text{ped}} = 0.40$ and 0.45 m. These sizes of pedestrians, combined with the aforementioned set of force parameters, allow reproducing of the two most important sets of macroscopic data satisfactorily.

4.2. Collision Avoidance

In this section, we explore the ability of the aforementioned models to reproduce microscopic (pairwise) and macroscopic collision avoidance. In particular, microscopic collision avoidance is focused on three different scenarios: a pedestrian walking towards an obstacle, two pedestrians walking towards each other in opposite directions, and a fast pedestrian overtaking a slower one. None of the three models include any algorithm to prevent collisions with obstacles, as in Ref. [31]; therefore, if we chose an initial impact parameter p, which is defined as the perpendicular distance between the path of the pedestrian and the center of the obstacle, equal to $p = 0$ m, pedestrians would either collide with or stop before the obstacle. Hence, we set the impact parameter equal to $p = 5$ cm in the starting position.

We use the force parameters of the model that best reproduced macroscopic empirical results. This is the asymmetric elliptical specification with $A = 60$ N and contact force parameters $H = 1.2\times10^4$ kg s^{-2} and $\gamma = 1.5\times10^4$ kg m^{-1} s^{-2}. The last two should be irrelevant if the model works well on the microscopic scale, and consequently, contact is avoided. As mentioned before, we study the effect of two other parameters: the relaxation time τ in the driving force and of ΔT from the elliptical specification.

In the macroscopic analysis, we calculate the time-average number of contacts per pedestrian for different values of the global density in the channel.

4.2.1. Pairwise Collision Avoidance

The desired velocity of pedestrians in macroscopic simulations is a Gaussian distribution with mean $v_0 = 1.45$ m/s. However, interactions among pedestrians occur with a relative velocity smaller than the desired one. Figure 12 shows the relative velocity of pedestrians (normalized by the mean desired speed v_0) as a function of the distance to other pedestrians (normalized by their diameter $D_{\text{ped}} = 0.5$ m) for $\rho = 1.0,\ 2.0,\ 3.0$ and 4.0 m^{-2}. The majority of interactions occur in the regime $v_{ij}/\langle v_0 \rangle \in [0, 0.25]$, which solving for v_{ij} gives relative velocities approximately between 0 and 0.3625 m/s. Therefore, we set the pedestrian-obstacle relative velocity to the highest value, $v_{ij} = 0.3625$ m/s.

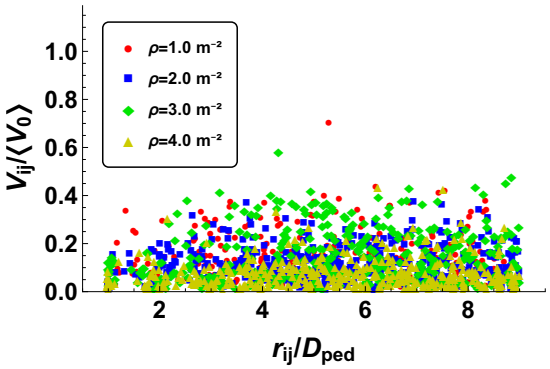

Figure 12: Relative velocity of interacting pedestrians, for different densities, as a function of the distance to the other pedestrian.

Figure 13 (a) shows the trajectory of a pedestrian avoiding an obstacle in the circular and elliptical specifications. In the regime of relative velocities that we are working on, both specifications successfully avoid contact. The difference between both models is slight, but the term $\mathbf{y}_{ij} = (\mathbf{v}_j - \mathbf{v}_i)\Delta T$ in the elliptical model introduces anticipation effect on the interaction; hence, pedestrians modify their trajectory earlier, and they deviate less from their original horizontal trajectory compared with the circular model.

In regards to the relaxation time τ, the deviation of pedestrians from their initial trajectory is inversely proportional to this parameter. Increasing the relaxation time reduces the driving force; hence, pedestrians will need more time to recover their desired velocity, and the deviation due to the interaction with the obstacle increases. In view of these results, the choice of $\tau = 1$ s done in the previous section (and common in the literature) seems correct as

it provides a not-exaggerated deviation of the pedestrian trajectory.

To see the effect of ΔT and the main difference between the circular and elliptical models, Figure 13 (b) shows the trajectories of two pedestrians walking in opposite directions and towards each other, with relative velocity $v_{ij} = 1.0$ m/s. We increased the relative velocity because; with the previous value of v_{ij}, the difference between models was inappreciable. With this new relative velocity, pedestrians collide in the circular specification and in the elliptical with $\Delta T = 1.0$ s, whereas if $\Delta T = 1.5$ s, collision is avoided, as each pedestrian feels the repulsion from the other before. Therefore, we conclude that the choice of the elliptical model over the circular is correct.

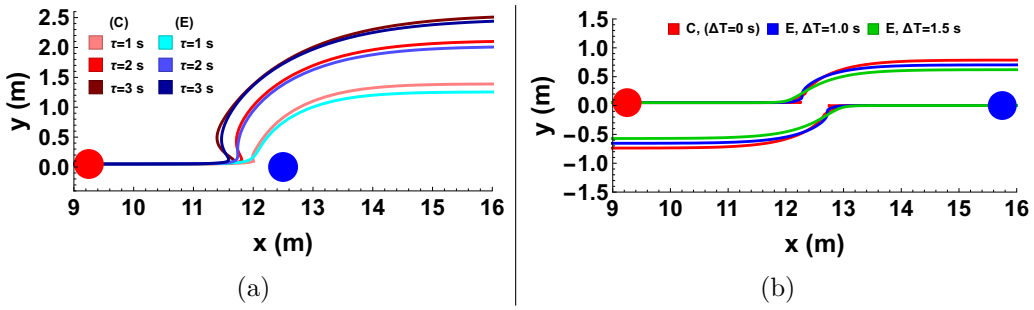

(a) (b)

Figure 13: Trajectories of pedestrians (red) in the circular (C) and elliptical (E) specifications, (a) avoiding an obstacle (blue), for different values of τ, with $v_{ij} = 0.3625$ m/s and with $\Delta T = 1$ s, and (b) avoiding another pedestrian (blue), for different values of ΔT, with $v_{ij} = 1.0$ m/s and $\tau = 1$ s.

As a final remark, we show the main difference between the symmetric and asymmetric elliptical specifications. For that purpose, we simulate two pedestrians walking in the same direction, with an initial impact parameter of $p = 5$ cm, and being the one in red faster than the one in blue. The former will overtake the latter, and the relative velocity is set to $v_{ij} = 0.2$ m/s to make the interaction last longer and visualize the differences between models better. Figure 14 (a) shows the trajectories for the elliptical case. Due to the symmetry in the interaction, the slower pedestrian steps aside as he/she feels the repulsion from the pedestrian behind and deviates from his/her original trajectory represented by the black dashed line. Since $\mathbf{f}_{ij}^r = -\mathbf{f}_{ji}^r$, they both feel the same repulsion and deviate approximately the same from the original $y = 0$ m.

Compared to the previous model, the asymmetric version in Figure 14 (b) shows a more realistic scenario. Now, it is the faster pedestrian who

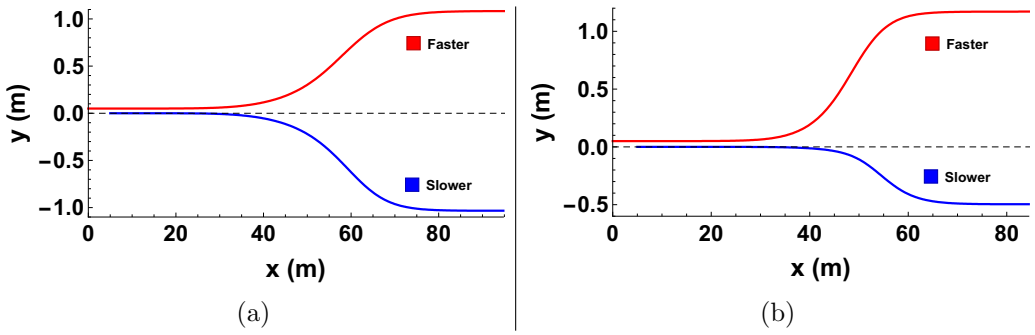

Figure 14: Trajectories of pedestrians when the faster, in red, overtakes the slower, in blue, in (a) the symmetric elliptical model, and (b) asymmetric elliptical model. The black dashed line represents the original straight path.

initially deviates and walks around the slower one in front. However, when they are side by side, the slower pedestrian starts to feel more strongly the repulsion, as it is less suppressed by the weight factor $w(\varphi_{ij})$, and as a result, he/she deviates half a meter from his/her original path. Still, there is an improvement with respect to the symmetric version.

In view of these results, the set of parameters that reproduced macroscopic results is capable of showing realistic collision avoidance in simple pedestrian-obstacle and pedestrian-pedestrian trajectories. In addition, we confirm that the value $\tau = 1$ s is adequate, that the elliptical specification offers a suitable anticipation for avoiding collisions, and that the asymmetric model produces more realistic trajectories than the symmetric one.

4.2.2. Macroscopic Collision Avoidance

In the previous subsection, we have shown that contact between pedestrians is successfully avoided in three specific scenarios. In those tests, only two pedestrians are considered, and they have enough space to avoid contact. However, in actual environments, pedestrian interactions are more complex since more than two people can be involved in interactions, which limits the amount of space that individuals have to avoid collisions, and the relative velocities can be higher than the v_{ij} that we have chosen. For this reason, we extend our analysis to the periodic corridor where the FD has been calculated. We consider the same force parameters as in the previous subsections, plus the $\Delta T = 1.5$ s and $D_{\text{ped}} = 0.45$ m, following the results from section 4.1.3. Using those parameters, we conduct simulations of pedestrian flows in the periodic corridor, with global pedestrian densities increasing from

$\rho = 0.5$ m^{-2} to maximum physical packing $\rho = 4.0$ m^{-2} in steps of 0.5 m^{-2}, using both the elliptical and the asymmetric elliptical models. In each time step, we calculate the number of contacts N_c per pedestrian (total number of contacts divided by the total number of pedestrians N_{ped}), and we calculate the time average for each value of the density.

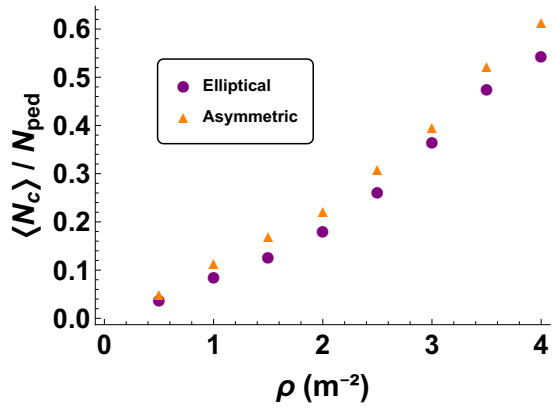

Figure 15: Average number of contact per pedestrian as a function of the global density.

Figure 15 shows the results for the two models. In both cases, the average number of contacts increases with the global density due to the decreasing free space in the corridor. Moreover, the average is not zero in any of the considered densities: in dilute scenarios, although there is more free space, the relative velocities of some pedestrians are high, as shown in Figure 12, whereas in congested cases, the lack of free space provokes an increase of the number of collisions. Furthermore, for densities above $\rho = 1.0$ m^{-2}, the model without limited visual range offers better collision avoidance. The weight function from eq. (5) limits the strength of the social force, which leads to more contacts happening in the asymmetric specification compared to the symmetric case.

5. Lane Formation in Bidirectional Pedestrian Flows

The last benchmark to assess the limited visual range in the social force model is a collective pattern of motion: lane formation (LF) in bidirectional pedestrian flows (BPF). To study the ability of simulated agents to form the lines, we isolate the system by removing walls and imposing periodic

boundary conditions in both the longitudinal and the transversal directions of the corridor. Moreover, we increase the size of the environment to $40\text{m} \times 15\text{m}$ so that pedestrians have enough space to accelerate to their desired velocity before the interaction with the counterflow happens. Agents are initially located in two waiting areas, those walking to the right are placed in random positions between $x \in [2.25, 9.75]$ m, while people walking to the left, in $x \in [30.25, 37.75]$ m, being in both cases the initial y-coordinate random between $y \in [0.25, 14.75]$ m.

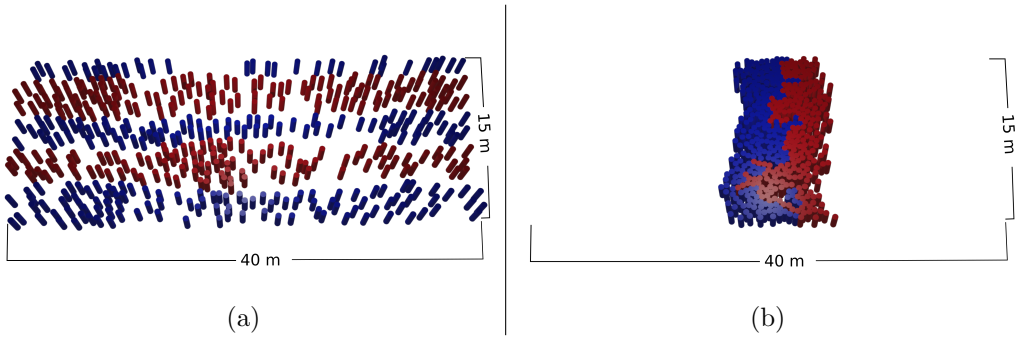

(a) (b)

Figure 16: (a) Lane formation in BPF for $\rho = 0.75$ m^{-2}. (b) Clogging in BPF for $\rho = 0.75$ m^{-2}.

The initial condition (snapshot in Figure 16) can affect the outcome of the simulation, i.e., having a stratification of pedestrian flows (Figure 16 (a)) or a clog (Figure 16 (b)). Therefore, following Ref. [37], we consider 10 random initial distributions of agents, and we calculate the probability of having line formation P_{LF}.

We repeat this procedure for several values of the global density to study to which extent the model works. Force parameters and pedestrian sizes are chosen as in section 4.2.2, and the desired velocities of the pedestrians are the normal distribution mentioned in section 3.1.

Figure 17 shows P_{LF} for densities between 0 and 1.08 m^{-2}. We reproduce lane formation in all cases up to $\rho = 0.75$ m^{-2}. At global densities $\rho = 0.75,\ 0.833$ and 0.916 m^{-2}, the probability drops, respectively, to 90 %, 30 % and 20 %, whereas for densities greater than $\rho = 1.0$ m^{-2}, the system clogs.

As the density increases, pedestrians collide more frequently with the oncoming group of agents. In the highest density scenarios, these collisions stop pedestrians, and a clog is formed. The clog lasts permanently, as the driving force of pedestrians can not overcome the social repulsion from the group of

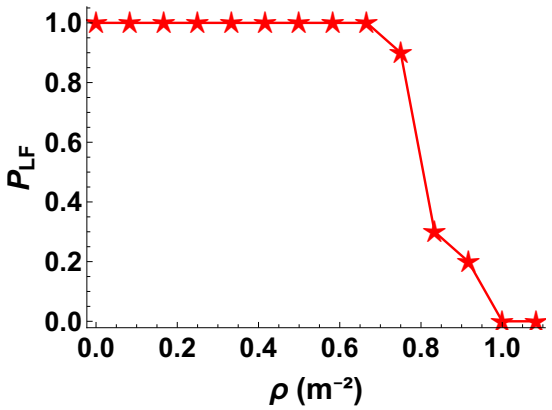

Figure 17: Lane formation in BPF as a function of the global density.

pedestrians in front, which has a local density much higher than 1.0 m^{-2}. In Ref. [37], they focus on jamming probability in BPF using three different models, being the best of them capable of reproducing lane formation up to $\rho = 1.5$ m^{-2}. Still, the critical density ρ_{crit} above which clogging occurs in bidirectional pedestrian flows is unknown; hence, experimental work is needed to validate numerical results.

6. Conclusion

We have studied the ability of the social force model to reproduce two of the most important sets of macroscopic empirical data: pedestrian flows through a bottleneck (BF) and the speed-density fundamental diagram (FD). We have shown the effect of each force parameter on the macroscopic dynamics: social force intensity accelerates the flow in symmetric specifications, as it reduces contact between pedestrians, whereas in the asymmetric model, social force intensity A slows the flow down as pedestrians feel a greater repulsion from all the obstacles above them. In both symmetric and asymmetric versions of the model, the greater compression H and smaller friction γ, the faster the flow, and vice-versa. Having said that, the effect of contact forces in channel flow is more noticeable in symmetric models, since friction is proportional to the relative velocity v_{ij} of pedestrians, which is considerably smaller in the asymmetric case due to the social force. We showed that results from the asymmetric elliptical specification reproduced experiments better than symmetric models, and we sought for a set of parameters to have a quantitative agreement. Then, we studied the effect of pedestrians' size in

macroscopic simulations using the calibrated asymmetric model. Reducing pedestrians' size decreases contacts among them, plus, it is easier for them to exit through the bottleneck, as they are smaller compared to the gate width; therefore, the BF is accelerated. On the other hand, since contact forces have a negligible effect on the channel flow, modifying pedestrians' size barely affects FD results. For pedestrian diameters $D_{\text{ped}} = 0.40$ and 0.45 m, our set of parameters can reproduce very well both BF and FD.

After the macroscopic study, we assessed the model for both pairwise and group collision avoidance. We focused on trajectories of pedestrians avoiding an obstacle either at rest or in motion. The impact parameter at the beginning of the simulation was $p = 0.05$ m, as the model does not include any algorithm to avoid the obstacle in case the p was zero. In the range of relative velocities that interactions occur in macroscopic simulations, the model showed collision avoidance in all tests. We have analyzed the effect of the relaxation time τ, which gives a bigger deviation from the initial path as it is increased since it is inversely proportional to the driving force. Then, we showed that the elliptical specification offers better collision avoidance than the circular, as it includes anticipation. In fact, for relative velocity $v_{ij} = 1.0$ m/s, we demonstrated that two pedestrians walking in opposite directions collide in the circular specification, but they may not touch in the elliptical if the anticipation time parameter ΔT is chosen great enough. Afterwards, we showed the advantages of asymmetric models over the symmetric one by simulating the trajectories of a pedestrian overtaking another one. In the symmetric case, both pedestrians deviated symmetrically from the original horizontal trajectory, whereas in the more realistic asymmetric model, it is the faster one that modifies strongly his/her trajectory to overtake the slower pedestrian. Subsequently, we calculated the average number of contacts per pedestrian in the channel flow. The average increases with the global density, as there is less free space to avoid each other, and the asymmetric model is slightly less effective than the symmetric in preventing collisions due to the suppression of the social force via the weight function $w(\varphi_{ij})$.

Nevertheless, the asymmetric model is more comprehensive than the elliptical, as it is able to reproduce the aforementioned BF and FD experimental results accurately. Finally, we studied the stratification of bidirectional pedestrian flows in a corridor with periodic boundary conditions in the two dimensions. Lane formation is reproduced up to moderately dense flow ($\rho \sim 0.75$ m^{-2}), whereas it is suppressed at higher densities where clogs are formed.

The asymmetric elliptical model with our set of parameters also has its limitations. As mentioned in the microscopic analysis, the model does not include any algorithm for collision avoidance, and if a pedestrian walked towards an obstacle with zero impact parameter, he/she would collide or stop in front of the obstacle, not avoid it. Nonetheless, this pathological condition in real simulations can be easily avoided by including a random noise force to slightly deviate pedestrians from the impact parameter $p = 0$ m path. On the other, the desired direction is predefined in our simulations. The geometry of the system was simple and a single predefined vector (pointing towards the bottleneck exit in BF simulations or parallel to the walls in FD and bidirectional pedestrian flow simulations) was sufficient to simulate the dynamics. In complex geometries, the model would require a different definition of the desired direction at every point of space. This will be the subject of further contributions.

Acknowledgements

This research is supported by the Basque Government through the BERC 2018-2021 programme and by the Spanish Government (AEI/FEDER) through BCAM Severo Ochoa excellence accreditation SEV-2017-0718. The authors also acknowledge the financial support received by the Basque Government through the "Mathematical Modeling Applied to Health" Project.

References

[1] D. Helbing, P. Molnár, Social force model for pedestrian dynamics, Phys. Rev. E 51 (1995) 4282–4286. doi:10.1103/PhysRevE.51.4282. URL https://link.aps.org/doi/10.1103/PhysRevE.51.4282

[2] D. Helbing, I. Farkas, T. Vicsek, Simulating dynamic features of escape panic, Nature 407 (2000) 487–490. doi:10.1038/35035023.

[3] A. Johansson, D. Helbing, P. K. Shukla, Specification of the social force pedestrian model by evolutionary adjustment to video tracking data., Advances in Complex Systems 10 (2007) 271–288. doi:10.1142/S0219525907001355.

[4] D. Helbing, A. Johansson, Pedestrian, Crowd and Evacuation Dynamics, Vol. 16, 2010, pp. 697–716. doi:10.1007/978-1-4419-7695-6_37.

[5] F. Zanlungo, T. Ikeda, T. Kanda, Social force model with explicit collision prediction, EPL (Europhysics Letters) 93 (2011) 68005. doi:10.1209/0295-5075/93/68005.

[6] I. Sticco, G. Frank, C. Dorso, Effects of the body force on the pedestrian and the evacuation dynamics, Safety Science 129 (2020) 104829. doi:10.1016/j.ssci.2020.104829.

[7] I. Sticco, G. Frank, C. Dorso, Social force model parameter testing and optimization using a high stress real-life situation, Physica A: Statistical Mechanics and its Applications 561 (2021) 125299. doi:10.1016/j.physa.2020.125299.

[8] M. Xu, Y. Wu, P. Lv, H. Jiang, M. Luo, Y. Ye, misfm: On combination of mutual information and social force model towards simulating crowd evacuation, Neurocomputing 168 (06 2015). doi:10.1016/j.neucom.2015.05.074.

[9] Y. Jiang, B. Chen, X. Li, Z.-j. Ding, Dynamic navigation field in the social force model for pedestrian evacuation, Applied Mathematical Modelling 80 (10 2019). doi:10.1016/j.apm.2019.10.016.

[10] Y. Han, H. Liu, Modified social force model based on information transmission toward crowd evacuation simulation, Physica A: Statistical Mechanics and its Applications 469 (11 2016). doi:10.1016/j.physa.2016.11.014.

[11] Z. Xin, F. Xin, M. Tai, Z. Xin, Improved social force model for emergency evacuation scene with limited field of vision, Journal of Physics: Conference Series 1769 (2021) 012046. doi:10.1088/1742-6596/1769/1/012046.

[12] R. Zhou, Y. Cui, Y. Wang, J. Jiang, A modified social force model with different categories of pedestrians for subway station evacuation, Tunnelling and Underground Space Technology 110 (2021) 103837. doi:10.1016/j.tust.2021.103837.

[13] W. Wu, M. Chen, J. Li, B. Liu, X. Wang, X. Zheng, Visual information based social force model for crowd evacuation, Tsinghua Science & Technology 27 (2021) 619–629. doi:10.26599/TST.2021.9010023.

[14] A. Schadschneider, A. Seyfried, Empirical Results for Pedestrian Dynamics and their Implications for Cellular Automata Models: Models, Data Collection and Applications, 2009, pp. 27–43. doi:10.1108/9781848557512-002.

[15] F. Dietrich, G. Köster, Gradient navigation model for pedestrian dynamics, Physical Review E 89 (2014) 062801. doi:10.1103/PhysRevE.89.062801.

[16] Y. Xiao, Z. Gao, Y. Qu, X. li, A pedestrian flow model considering the impact of local density: Voronoi diagram based heuristics approach, Transportation Research Part C: Emerging Technologies 68 (2016) 566–580. doi:10.1016/j.trc.2016.05.012.

[17] T. Rupprecht, W. Klingsch, A. Seyfried, Influence of Geometry Parameters on Pedestrian Flow through Bottleneck, 2011, pp. 71–80. doi:10.1007/978-1-4419-9725-8_7.

[18] W. Liao, A. Seyfried, J. Zhang, M. Boltes, Z. Xiaoping, Y. Zhao, Experimental study on pedestrian flow through wide bottleneck, Vol. 2, 2014. doi:10.1016/j.trpro.2014.09.005.

[19] K. Müller, Zur gestaltung und bemessung von fluchtwegen für die evakuierung von personen aus bauwerken auf der grundlage von modellversuchen. dissertation, technische hochschule magdeburg (01 1981).

[20] X. Liu, W. Song, W. Lv, Empirical data for pedestrian counterflow through bottlenecks in the channel, Transportation Research Procedia 2 (12 2014). doi:10.1016/j.trpro.2014.09.006.

[21] T. Kretz, A. Grünebohm, M. Schreckenberg, Experimental study of pedestrian flow through a bottleneck, Journal of Statistical Mechanics: Theory and Experiment (2006) P10014doi:10.1088/1742-5468/2006/10/P10014.

[22] A. Seyfried, O. Passon, B. Steffen, M. Boltes, T. Rupprecht, W. Klingsch, New insights into pedestrian flow through bottlenecks, Transport. Sci. 43 (2007) 395–406. doi:10.1287/trsc.1090.0263.

[23] R. Nagai, M. Fukamachi, T. Nagatani, Evacuation of crawlers and walkers from corridor through an exit, Physica A-statistical Mechanics and Its Applications - PHYSICA A 367 (2006) 449–460. doi:10.1016/j.physa.2005.11.031.

[24] H. Muir, D. Bottomley, C. Marrison, Effects of motivation and cabin configuration on emergency aircraft evacuation behavior and rates of egress, International Journal of Aviation Psychology - INT J AVIAT PSYCHOL 6 (1996) 57–77. doi:10.1207/s15327108ijap0601_4.

[25] B. Hankin, R. Wright, Passenger flow in subways, Journal of The Operational Research Society - J OPER RES SOC 9 (1958) 81–88. doi:10.1057/jors.1958.9.

[26] J. Zhang, W. Klingsch, A. Schadschneider, A. Seyfried, Transitions in pedestrian fundamental diagrams of straight corridors and t-junctions, Journal of Statistical Mechanics: Theory and Experiment 2011 (2011) P06004. doi:10.1088/1742-5468/2011/06/P06004.

[27] M. Mōri, H. Tsukaguchi, A new method for evaluation of level of service in pedestrian facilities, Transportation Research Part A: General 21 (1987) 223–234. doi:10.1016/0191-2607(87)90016-1.

[28] S. Older, Movement of pedestrians on footways in shopping streets, Traffic Eng Contr 10 (11 1967).

[29] U. Weidmann, Transporttechnik der fugänger, Schriftenreihe des Institut für Verkehrsplanung, Transporttechnik, Straen- Und Eisenbahnbau 78 (1993) 62–64.

[30] L. Vanumu, K. R. Rao, G. Tiwari, Fundamental diagrams of pedestrian flow characteristics: A review, European Transport Research Review 9 (12 2017). doi:10.1007/s12544-017-0264-6.

[31] D. Parisi, M. Gilman, H. Moldovan, A modification of the social force model can reproduce experimental data of pedestrian flows in normal conditions, Physica A: Statistical Mechanics and its Applications 388 (2009) 3600–3608. doi:10.1016/j.physa.2009.05.027.

[32] E. Bassoli, L. Vincenzi, Parameter calibration of a social force model for the crowd-induced vibrations of footbridges, Frontiers in Built Environment 7 (05 2021). doi:10.3389/fbuil.2021.656799.

[33] M. Chraibi, A. Seyfried, Pedestrian dynamics with event-driven simulation (07 2008). doi:10.1007/978-3-642-04504-2_69.

[34] M. Moussaïd, D. Helbing, G. Theraulaz, How simple rules determine pedestrian behavior and crowd disasters, Proceedings of the National Academy of Sciences of the United States of America 108 (2011) 6884–8. doi:10.1073/pnas.1016507108.

[35] I. Karamouzas, B. Skinner, S. Guy, Universal power law governing pedestrian interactions, Physical review letters 113 (12 2014). doi:10.1103/PhysRevLett.113.238701.

[36] A. Seyfried, B. Steffen, T. Lippert, Basics of modelling the pedestrian flow, Physica A: Statistical Mechanics and its Applications 368 (07 2005). doi:10.1016/j.physa.2005.11.052.

[37] Q. Xu, M. Chraibi, A. Seyfried, Anticipation in a velocity-based model for pedestrian dynamics, Transportation Research Part C: Emerging Technologies 133 (2021) 103464. doi:10.1016/j.trc.2021.103464.

[38] M. Chraibi, A. Seyfried, A. Schadschneider, Generalized centrifugal force model for pedestrian dynamics, Physical review. E, Statistical, nonlinear, and soft matter physics 82 (2010) 046111. doi:10.1103/PhysRevE.82.046111.

[39] A. Forde, J. Daniel, Pedestrian walking speed at un-signalized midblock crosswalk and its impact on urban street segment performance, Journal of Traffic and Transportation Engineering (English Edition) 8 (2020) 57–69. doi:10.1016/j.jtte.2019.03.007.